''Nonrelativistic'' ionization of the *L*-shell states in argon by a ''relativistic'' 10^{19} W/cm^2 laser field

Enam A. Chowdhury,[1] C. P. J. Barty,[2] and Barry C. Walker[1]
[1]*Department of Physics and Astronomy, University of Delaware, Newark, Delaware 19716*
[2]*Department of Chemistry and Biochemistry, University of California San Diego, San Diego, California 92093*
(Received 21 September 2000; published 20 March 2001)

The field ionization cross sections for the *L*-shell states in argon are presented as measured with pulsed-laser radiation at an intensity of up to 10^{19} W/cm^2. For ultrahigh intensities, the photoelectron continuum dynamics will be relativistic. However, the measured charge-state yields for Ar^{9+} to Ar^{16+} compare favorably to numerical solutions of the nonrelativistic Schrödinger equation and a widely used Ammosov-Delone-Krainov/WKB tunneling ionization model. The results are interpreted within a two-step, strong-field ionization model, where the initial tunneling ionization process is dominated by nonrelativistic effects while the photoelectron continuum dynamics are strongly relativistic.

DOI: 10.1103/PhysRevA.63.042712 PACS number(s): 32.80.Fb, 32.80.Rm, 52.25.Jm, 52.80.−s

I. INTRODUCTION

Extensions of the field-matter interaction into the relativistic regime, such as recently with multiphoton Compton scattering [1] and the angular emission of electrons [2], depend upon understanding the ultrahigh field ionization mechanism. Several relativistic phenomena resulting from ultrahigh field-atom interactions have been predicted. These include Larmor radiation, differences in the energy-resolved photoionization cross section, and the stabilization [3–5] of an atom against field ionization. However, many aspects of the relativistic field-atom interaction are not known because approximations within models can fail at relativistic intensities [6]. Furthermore, it has remained experimentally unclear how even basic physical quantities, such as the photoionization cross sections, are modified in the relativistic domain.

We present here the fundamental, single-atom photoionization cross sections for argon in a field with an intensity range from 10^{18} W/cm^2 to 10^{19} W/cm^2. These measurements quantify the atomic ionization rates for field strengths of 100 GV/cm and quantify the field ionization of atomic inner shell states as high as Ar^{16+}.

II. EXPERIMENT

The laser system we used to generate an irrandiance of 10^{19} W/cm^2 is described in [7]. This laser system is the most recent generation of the terawatt class. Previous terawatt laser systems were based on a glass amplification medium. The single-shot operation of these lasers allowed ultrahigh field plasma studies [8,9] but hindered ultrahigh intensity studies of atomic systems. Our laser system has a repetition rate of 10 Hz and pulse-energy fluctuations of 5%. This performance allows ultrahigh intensity atomic measurements to be made accurately over a high dynamic range. Briefly, the system is a four-stage Ti:sapphire chirped pulse amplifier system that produces linearly polarized pulsed radiation with a pulse energy of 1.2 ± 0.06 J, a duration of 25 ± 5 fs, and a center frequency of 800 nm. The pulse is temporally compressed in a vacuum of 10^{-6} Torr and then enters an ultrahigh vacuum interaction region via a 11-cm-diameter, 5-μm-thick antireflection-coated nitrocellulose pellicle. Two high-compression turbo pumps in series evacuate the high-intensity interaction region to a base pressure of less than 40 pTorr. In the interaction chamber, the laser pulses are focused by a 11-cm-diameter, $f/2.5$, metal off-axis parabolic mirror. Approximately 40% of the laser-pulse energy is delivered within a 3-μm-diameter focal spot. The dominant focal aberration is chromatic that results in an estimated reduction of the focused intensity by a factor of 2. The pulse duration, spot size, and integrated pulse energy optical measurements give an intensity calibration in the laser focus of 10^{20} W/cm^2 for every joule of energy in the laser pulse.

Ultrahigh purity ($>99.999\%$) sample gases of helium, neon, and argon are introduced to the focal region in a skimmed, effusive gas jet whose diameter at the focus is approximately 0.25 mm. The gas pressure in focal region is varied from 10^{-5} Torr to 10^{-8} Torr. The ion products from the laser-matter interaction region are swept into a one-meter time-of-flight tube by a 200-V potential. Microchannel plates (MCP) are used to detect the fragments. The MCP signals were amplified and discriminated with a combination constant fraction/threshold discriminator. To avoid bleaching of the MCP detector area with high detector currents from low charge state species ($q<2$), the MCP was operated with low gain. The MCP/amplifier/discriminator detection system was set for optimal detection efficiency for m/q ratios less than 5. Tests of the MCP response as a function of the gain voltage and incident charge species were done. The variance in experimental detection sensitivity for Ar^{8+} to Ar^{14+} argon species was 20%.

To calibrate the laser intensity with greater accuracy than the calibration inferred from the independent optical measurements, we record known intensity-dependent ionization rates in the laser focus of the experiment. The ionization rates of helium are the highest-intensity measurements available with a cross section shown reliable to an accuracy of 15% over a large signal range [10]. The experimental and calculated photoionization yields for helium ionized by a 25-fs pulse of 800-nm radiation are shown in Fig. 1. The number of detected ions (normalized to the pressure in Torr)

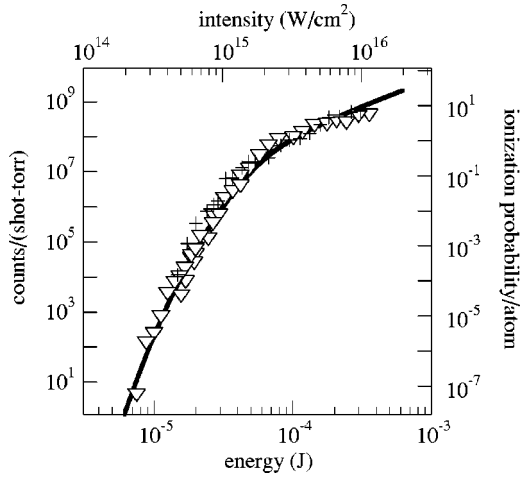

FIG. 1. Experimental and calculated photoionization yields for helium ionized by a 25-fs pulse of 800-nm radiation. Data collected with the 0.2-J laser preamplifier (∇) and full 1.2-J amplification ($+$) are shown. The intensity to energy calibration is obtained by fitting the experimental measurements to the calculated yields (solid line).

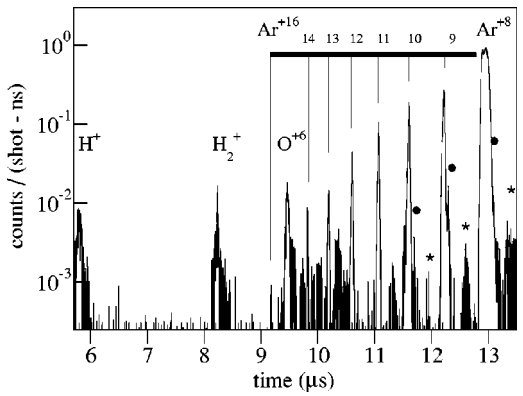

FIG. 2. Time-of-flight ion spectrum for argon at the intensity 2×10^{19} W/cm^2. The tie bars identify $_{18}Ar^{40}$ while the isotopes $_{18}Ar^{38}$ and $_{18}Ar^{36}$ are identified by $*$ and ●, respectively. The contaminants H and O are also labeled in the figure. The Ar^{8+} species is saturated.

is plotted as a function of the pulse energy. This data was fit with the calculated ionization yield [11] by adjusting the energy to intensity calibration and ion yield. The measurements were collected with pulses from the 0.2-J laser preamplifier and the 1.2-J amplifier. The agreement between the 0.2-J and 1.2-J data indicates that laser amplifier distortions were not significant in the experiment. The intensity calibration measured with the photoionization of helium shown in Fig. 1 is 3.2×10^{19} W/cm^2 at the focus per joule of energy in the laser pulse. The estimated uncertainty of the photoionization yield intensity calibration is 60%. We believe that cumulative or undetected optical errors in the convoluted optical measurements are responsible for the disagreement between the photoionization yield calibration and the higher optical estimate. The factor-of-3 disagreement between the intensity calibration using photoionization and that inferred from optical measurements emphasizes the need for accurate quantification of ultrahigh intensities in the interaction region, just as has been the case for previous high-field studies. The peak intensity achieved in these studies was $2.0\pm1.2\times10^{19}$ W/cm^2 according to the helium photoionization calibration with 0.62 J of energy in a pulse duration of 25 ± 5 fs delivered to the interaction region.

For peak intensities approaching 10^{19} W/cm^2 the valence and inner shell electrons of many atoms will be fully ionized. However, the L shell of argon is ideally suited for atomic studies in the intensity range from 10^{18} W/cm^2 to 10^{19} W/cm^2 since the L-shell ionization potentials extend from 422 V to 918 V. Furthermore, argon's M-shell valence electrons ionize at much lower intensities, so Ar^{8+} is a clean high-field ion ground state unencumbered by possible multielectron dynamics from valence shell electrons. The ionization of Ar through Ar^{7+} occurs over the intensity range of 2×10^{14} W/cm^2 to 3×10^{16} W/cm^2. The third-order autocorrelation of our experimental pulse shows the intensity of 10^{15} W/cm^2 is reached 270 fs before the peak of the pulse, 10^{16} W/cm^2 is reached 190 fs before the peak of the pulse. The measured photoionization yield at 2×10^{19} W/cm^2 is shown in Fig. 2. Tie bars are used to show the peaks for the dominant isotope of argon. Ar^{15+} is not visible due to the $O^{6+}\rightarrow O^{7+}$ (ionization potential 138 V$\rightarrow$739 V) transition from residual ionized water in the chamber. The background in the experiments does not otherwise encumber the studies due to the very low level of detected H^+, H_2^+, and a lack of degenerate m/q ratios for other argon charge states. The event rates for Ar^{9+} to Ar^{16+} were kept below 0.25/(bin-shot) to prevent pulse pileup. Figure 2 is the sum average of 20 000 shots. The sample pressure was varied in the experiments to verify the absence of collective effects.

III. THEORETICAL ANALYSIS

Several gauges of the atom-field interactions can be used to analyze the observed ultrahigh intensity ionization yields. Perhaps the most fundamental of these is the Keldysh parameter, γ is equivalent to field frequency/tunneling frequency [12], which relates the radiation time scale to the tunneling ionization-time scale. The Keldysh parameter for these studies averages 0.03. The slowly varying ionizing field relative to the tunneling rate in these experiments is consistent with a predominantly quasistatic dc field ionization, which has been verified for γ values as high as 0.5 [10].

More than 30 years ago, Landau [13] used a semiclassical method, also known as WKB, to obtain the dc field ionization rates for hydrogen. Smirnov and Chibisov [14] and Perelomov *et al.* [15] later devised a way to apply this approximation to hydrogenic atomic states of different atoms. Following Landau, these derivations used a parabolic cylindrical coordinate representation of the Schrödinger equation with the atomic state approximated with a single active electron hydrogenic state under the influence of a dc field. With an electric field along the z axis, electron dynamics may be separated along $\xi=r+z$, and $\eta=r-z$ parabolic axes. The two separated equations can be rendered in a form identical to a one-dimensional Schrödinger's equation. Since electron ionization occurs predominantly on one side of the atom or

TABLE I. Criteria for evaluating the validity of the WKB approximation along the η coordinate for the L states of argon or K state of helium. The field strengths F used are the average of those in Table II for each species. The extent of the wave function is approximated by $Ze^2/2E$ and twice the ratio of the bound energy to the external potential is given by $2E/eF$.

Species Z	$Ze^2/2E$ (Å)	Barrier start (Å)	Barrier end (Å)	$2E/eF$ (Å)
2	0.27	0.72	5.0	5.6
9	0.15	0.58	3.1	3.6
14	0.13	0.50	2.5	3.0
16	0.13	0.49	2.4	2.8

ion, where the electric field has suppressed the barrier, only one of these two coordinates is of interest and the equation reduces to a one-dimensional barrier penetration problem. The general atomic wave function is expressed in parabolic coordinates as $\Psi(r,\theta,\phi)=\zeta(\xi)\chi(\eta)\Phi(\phi)/\sqrt{\xi\eta}$, where ϕ is the usual azimuthal angle. The separated equation for η becomes

$$\frac{d^2}{d\eta^2}\chi(\eta)+\frac{m_e}{\hbar^2}\left(\frac{E}{2}+\frac{ke^2\beta_2}{\eta}+\frac{\hbar^2}{4m_e\eta^2}+\frac{eF\eta}{4}\right)\chi(\eta)=0, \tag{3.1}$$

where E is the bound state energy of the electron of mass m_e and charge e. The separation constants for $\zeta(\xi)$ and $\chi(\eta)$ are β_1 and β_2, respectively, where $\beta_1+\beta_2=Z$, the charge of the ion. The terms $ke^2\beta_2/\eta$ and $\hbar^2/4m_e\eta^2$ represent the Coulomb potential. F is the electric field, and k is $1/(4\pi\epsilon_0)$ for MKSA units. The WKB method begins by assuming certain characteristics about the tunneling wave function. For the wave function entering the barrier, the asymptotic field-free radial atomic wave function is used. This amounts to an assumption the barrier is far from the core, i.e., $Ze^2/(2E) \ll \eta$ where Z is the charge of the ion final state. A second approximation requires the potential in the region of the barrier, due to the external field, is much less than the energy of the electron, i.e., $\eta \ll 2E/eF$. In a classical sense, this will mean the electron will experience no significant acceleration, which would change its kinetic energy, until into the continuum and well outside the barrier. If these conditions hold, then the WKB wave function inside the barrier can be obtained and matched to the asymptotic continuum wave function. Table I summarizes these criteria for the ionization of the argon charge states studied. From Table I, it is apparent the WKB inequality relationships are satisfied by a factor of 3. When the electron is presupposed to be in an atomic state with quantum numbers n^*, l^*, m, the often-used Ammosov-Delone-Krainov [11] rate is obtained. This formula has been used to describe a broad range of interactions from hydrogen in microwave fields [16] to diatomic molecules in femtosecond laser fields [17]. By comparing the WKB/Ammosov-Delone-Krainov (ADK) solution with numerical solutions to the Schrödinger equation and experimental measurements, we will demonstrate whether it is justified to invoke these approximations in ultrahigh-field interactions with inner shell states.

Numerical [18] and power series basis set expansion [19] methods were used to calculate the tunneling rate through the barrier using the Schrödinger equation in parabolic coordinates. We calculated the ionization for argon's bound states as represented by purely hydrogenic (n,l,m) states and the empirically adjusted n^*,l^*,m states [11]. When comparing between methods, we present here the analysis of $m=0$ states since they all have the same form in parabolic cylindrical representation. Among the possible states of the L shell in argon, $\mathrm{Ar}(1s^22s^22p^6)^{8+}$, $\mathrm{Ar}(1s^22s^22p)^{13+}$, and $\mathrm{Ar}(1s^22s)^{15+}$, were selected as representative of the ionization physics. The solutions were compared for ionization rates of order 10^{10}/s to 10^{13}/s. The numerical solutions were propagated well outside the barrier (more than 100 atomic radii), with a local error tolerance of 10^{-12}. We used standard techniques of elementary one-dimensional barrier penetration to rule out unphysical solutions. As an initial condition, the lowest η value in the solution was set to 0.2% of the radial expectation value of the bound state. This boundary condition was motivated by the fact that the Coulomb field is much greater than the external field near the core and the wave function should therefore be least perturbed from the field-free solution. The equation was then solved and the converged solution to the equation was used to calculate the tunneling rate. Also, to check for consistency asymptotically, this equation was converted to the Airy's equation by an affine transformation. The solutions were then computed with standard subroutines and compared against the physical solution family well outside the barrier. They were in excellent agreement with each other. Outside the barrier, the solutions are oscillating functions with an amplitude scaling as the square root of the momentum and a slowly varying frequency. We also calculated power series solutions to the same equation. These were in excellent agreement with the numerical solutions over their range of validity. Because the wave function is oscillating, a large number of terms needs to be retained to keep accuracy of solutions. In the case of He^+, to achieve convergence up to 7 Å, 70 terms needed to be used. The wave function $\chi(\eta)$ for $\mathrm{Ar}(1s^22s^22p)^{13+}$ for an ionization rate of 10^{13}/s is shown in Fig. 3. In this case, despite the high-field intensity and large binding energy of the ionizing state, the WKB approximation should be valid and accurately represent the physics of the ionization process.

The calculations of the dc tunneling ionization rate using the various methods are summarized in Table II for hydrogenlike, single electron, L-shell states in argon. Two semiclassical analysis methods are shown in the table. The derived ADK rates, which include the coefficients $C_{n^*l^*}$ and our own WKB solution to the Schrödinger equation. The differences between these two rates can be tied to the analytical coefficient $C_{n^*l^*}$ used to match the bound to continuum wave function in the ADK solutions. Our WKB solutions are otherwise very much like the ADK wave function. The numerical solutions to the Schrödinger equa-

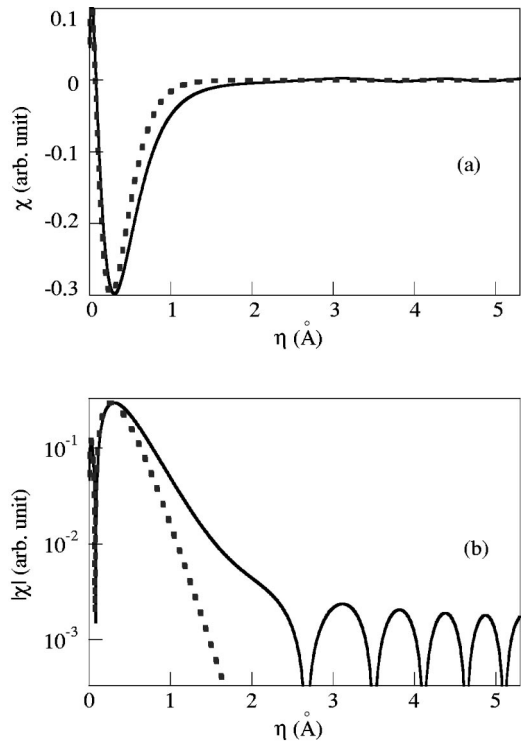

FIG. 3. The χ wave function for $Ar(1s^2 2s^2 2p)^{13+}$ for an ionization rate of 10^{13}/s is shown (solid line) along the η coordinate. The field strength (intensity) is 5.6×10^{10} V/cm (4×10^{18} W/cm^2). Also shown is the field free atomic wave function for $Ar(1s^2 2s^2 2p)^{13+}$ (dash line). The χ wave function is shown in (a) and the absolute value, $|\chi|$, is semilogarithmically plotted in (b).

tion are very close to the WKB and ADK rates though they are slightly higher on average than either the ADK or WKB rates.

For comparison, the dc ionization rates were also calculated using a perturbative theoretical technique derived by Silverstone *et al.* [20] for the ionization of hydrogenic states. This calculated rate for the ionization of hydrogenic $Ar(1s^2 2s)^{15+}$ at a field of 5.3×10^{10} V/cm is 1.1×10^{9} s and may be compared to the other values in Table II.

TABLE II. dc ionization rates for selected states of argon. Helium is also shown for reference. Hydrogenic states, noted by subscript H, use integer nlm quantum numbers while scaled hydrogenic states use fractional n^*l^*m states. NSE represents the results from numerically integrating the Schrödinger equation.

Z	Field	ADK		WKB	NSE
Ion	(V/cm)	$\lvert C_{n^*l^*}\rvert^2$	1/s	1/s	1/s
2_H	1.9×10^9	4.0	1.0×10^{13}	1.0×10^{13}	1.1×10^{13}
9_H	9.7×10^9	1.3	1.7×10^{10}	1.7×10^{10}	2.1×10^{10}
	1.3×10^9		1.1×10^{13}	1.1×10^{13}	1.3×10^{13}
14_H	3.6×10^{10}	1.3	2.5×10^{10}	2.5×10^{10}	3.1×10^{10}
	4.5×10^{10}		1.0×10^{13}	1.0×10^{13}	1.3×10^{13}
16_H	5.3×10^{10}	4.0	1.8×10^{10}	1.8×10^{10}	2.3×10^{10}
	6.7×10^{10}		1.0×10^{13}	1.0×10^{13}	1.3×10^{13}
9	2.1×10^{10}	2.3	8.1×10^{10}	3.8×10^{10}	6.1×10^{10}
	2.7×10^{10}		2.7×10^{13}	1.3×10^{13}	2.0×10^{13}
14	4.5×10^{10}	1.6	4.9×10^{10}	3.8×10^{10}	5.1×10^{10}
	5.7×10^{10}		1.4×10^{13}	1.1×10^{13}	1.4×10^{13}
16	5.7×10^{10}	4.1	1.1×10^{10}	1.0×10^{10}	1.3×10^{10}
	7.4×10^{10}		1.1×10^{13}	1.1×10^{13}	1.4×10^{13}

Questions about the validity of the nonrelativistic approximation used when formulating the Schrödinger equation for the interaction of ultrahigh intensities with high-energy bound states can be addressed by evaluating two aspects of the problem. If one considers the field-free approximation to the initial state and neglects the magnetic force from the field, then an additional criteria for a WKB analysis is the semiclassical condition for the wave function near the barrier. We have compared the semiclassical constraint for the barrier penetration problem [13] in argon ($n=2$) and hydrogen ($n=2$) for field strengths with significant tunneling ionization, i.e., Coulomb/laser field ≈15. We determined that hydrogen and the L-shell states $Ar(1s^2 2s^2 2p^6)^{8+}$ to $Ar(1s^2 2s)^{15+}$, all approach the barrier with nearly the same semiclassical constraint parameter.

When the Lorentz force from the external field is considered, it is likely that nonrelativistic approximation will not accurately represent the interaction of the bound state with the external field. A new aspect of the ionization dynamics should occur. For the Ar $(1s^2 2s)^{15+}$ state in these experiments, the $\mathbf{v}\times\mathbf{B}$ force on the electron is significant since $|\mathbf{v}/c|$ for the bound state electron is approximately 0.07. This Lorentz force, which for linear polarization can accelerate the electron in the propagation direction, will alter the ionization probability off the axis of the electric field. Whether or not ultrahigh fields can modify the ionization process via the magnetic force on the initial state is a question of the electron dynamics. As higher and higher energy bound states are ionized by ultrastrong fields, the increase in the $\mathbf{v}\times\mathbf{B}$ force will make such phenomena more pronounced. Some aspects of these high $\mathbf{v}\times\mathbf{B}$ forces should be mentioned. At the peak of the potential barrier, the electric field is zero while the magnetic field is at a maximum. Furthermore, the cyclotron frequency for bound-state electrons in fields with intensities of 10^{19} W/cm^2 to 10^{20} W/cm^2 is much greater than the 0.4-PHz laser frequency often used in high field experiments. Such an interaction may suppress ionization as the electron is ''deflected'' from ionizing along the electric field. In these studies, though the rates are lower than expected from the intensity calibration, the total ionization rate is not beyond the experimental error. Theoretical studies are currently underway to study this topic. Experimental studies of the energy-resolved photoelectron yield could be more sensitive to such relativistic effects [21,22].

IV. DISCUSSION

The agreement between the WKB, ADK, and numerical solutions, for the dc field ionization rate is high. The comparison between the experimental ionization yields and the calculated yields using these rates answers the validity of the common assumptions within the models. To compare to the experiments, the calculated yields were spatially and tempo-

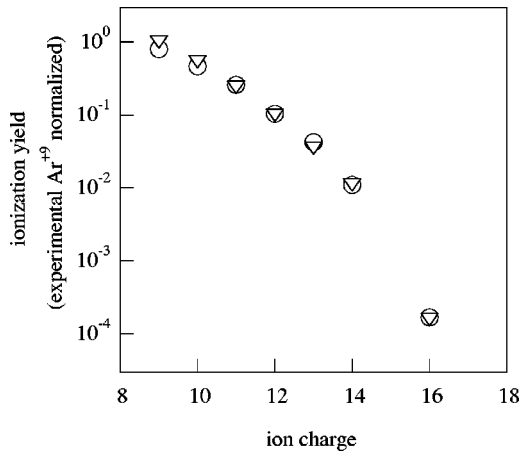

FIG. 4. Plot of experimental (∇) ion yields at an intensity of 2×10^{19} W/cm^2 and calculated ionization probability scaled to the experimental yield ($\bigcirc$) at 0.8×10^{19} W/cm^2. The yields have been normalized relative to the experimental yield of Ar^{9+}.

rally integrated using a gaussian focus and a $\cos^2$ pulse envelope.

In order to characterize the degree of agreement or disagreement, we analyzed the deviation between the experimental and theoretical charge state distributions over the range of the experimental uncertainty in the field intensity and the gas density. The best agreement is a minimum in the sum of squares deviation between the calculated and the experimental Ar^{9+} to Ar^{14+} and Ar^{16+} charge-state distribution. The deviation of each ion in the distribution was normalized to the charge state yield to avoid biasing the fit with the higher yield, low-charge ions in the charge-state distribution. In addition, the sum of squares was calculated by weighting each ion yield in the charge distribution by its statistical and experimental uncertainty.

The best agreement between the calculated and experimental yields occurs when using a theoretical intensity of 0.8×10^{19} W/cm^2 (which is at the lower bound for the experimental intensity uncertainty.) This lower bound in the possible experimental intensity is consistent with our ionization measurements of the *K* shell of neon. At an intensity of 2×10^{19} W/cm^2 the calculated semiclassical tunneling ionization probability for the Ne $1s^2$ state is 0.001%, at 2.5×10^{19} W/cm^2 the ionization probability for this state is 0.3%. Since no significant ionization of the *K* shell in neon could be observed in experiments at the intensity of $(2\pm1.2)\times10^{19}$ W/cm^2 and an event probability detection limit near 10^{-5}, the actual experimental intensity may be towards the lower bound of the calibration range.

For the case of best agreement, Fig. 4 compares the ionization yields for the species Ar^{9+} to Ar^{14+} and Ar^{16+} as calculated using the ADK model of ionization. Across all the charge states, the agreement in the yields is very good. For the charge state Ar^{16+}, where relativistic effects are expected to be most pronounced, the estimated one-sigma experimental uncertainty in the yield of Ar^{16+} is $\pm60\%$. One may infer from the agreement between the measurements and the calculated ionization rates, for example, the ultrahigh field, single electron ionization process at field strengths of 100 GV/cm for the ionization of the 2*s* state in argon is quasistatic and semiclassical. These measurements reveal an important aspect of the strong field photoionization process. At ultrahigh experimental intensities the photoelectron continuum dynamics are relativistic; the peak kinetic energy for an electron in the experimental field ranges from 0.1 MeV to 0.8 MeV. However, relativistic effects that might be expected to play a leading part in the fundamental ionization process, are not pronounced in these studies.

To resolve this paradox, one can consult classical [23] and two-step models [24] of strong field ionization first conceived for ionization at field strengths of less than one atomic unit. In step one of these models, the atom is ionized by the strong field, e.g., via the tunneling mechanism. In the second step, the dynamics of the ionized electron are dominated by the strong, oscillating electromagnetic field, which may cause rescattering of the continuum electron with the parent ion [25]. For the experiments considered here, the physics of step one has remained nonrelativistic whereas the dynamics of step two, most of which have yet to be seen, will likely be relativistic. Experiments at field intensities of 5×10^{17} W/cm^2 already manifest such continuum relativistic effects [26]. The measured ionization cross section, i.e., ''step one'' of ionization, does not significantly deviate from nonrelativistic models of ionization up to Ar^{16+}. These observations are consistent with the measurements made at lower intensities on Ne^{8+} where the initial kinetic energy of electron just after ionization was measured to be 0.2% of the energy of the electron in the continuum, a maximum of 25 keV in [27].

Although our calculations neglect multielectron ionization phenomena, our measurements have been done near or well above the saturation point of the single ionization process. Previous nonrelativistic, strong-field multielectron studies have shown that multielectron ionization rates are less than a few percent of the single electron rate [28]. Therefore, unless this trend is reversed for the relativistic continuum case, multielectron phenomena will not significantly contribute to the ionization yields measured in our experiment. The difference between adjacent observed charge-state yields is not of the order of a few percent. The yield of Ar^{14+}, for example, is 29% that of Ar^{13+}. Therefore, double ionization would have to account for roughly 10% of the total ionization yield to skew the results. We would like to emphasize the agreement in Fig. 3(b), best stated as a relative agreement between the charge states and the calculated rates. To better define the experimental results, absolute and energy-resolved rate measurements are necessary and such experiments are currently underway.

V. CONCLUSION

We have measured and calculated the photoionization yields for the *L* shell of argon with 10^{-14}-s pulses at a field (intensity) of 100 GV/cm (10^{19} W/cm^2). The observed rates are in good agreement with the nonrelativistic tunneling rates calculated using numerical and WKB solutions to the non-

relativistic Schrödinger equation. Within a ''two-step'' model of ionization, the results show that ''step one'' of the ionization process is nonrelativistic at ultrahigh fields. These experiments extend the general intensity domain for a well-known ADK/WKB tunneling model of strong-field optical atomic ionization up to interaction intensities of 10^{19} W/cm^2. Despite the expected prominence of relativistic effects in ''step two'' of the ionization process at the experimental intensities, higher field strengths are required to observe relativistic effects in the first ''ionization step'' of the field-atom ionization process.

ACKNOWLEDGMENTS

The authors gratefully acknowledge the support of Professor Kent R. Wilson. The experimental measurements were conducted at the Wilson Laboratory at the University of California San Diego. Funding for the studies was provided in part by the University of Delaware.

[1] C. I. Moore, J. P. Knauer, and D. D. Meyerhofer, Phys. Rev. Lett. **74**, 2439 (1995).
[2] S. J. McNaught, J. P. Knauer, and D. D. Meyerhofer, Phys. Rev. Lett. **78**, 626 (1997).
[3] R. Taieb, V. Veniard, and A. Maquet, Phys. Rev. Lett. **81**, 2882 (1998).
[4] J. Grochmalicki, M. Lewenstein, and K. Rzazewski, Phys. Rev. Lett. **66**, 1038 (1991); K. C. Kulander, K. J. Schafer, and J. L. Krause, *ibid.* **66**, 2601 (1991).
[5] C. J. Joachain, M. Dorr, and N. Kylstra, Adv. At., Mol., Opt. Phys. **42**, 225 (2000).
[6] J. W. Braun, Q. Su, and R. Grobe, Phys. Rev. A **59**, 604 (1999).
[7] B. C. Walker, C. Toth, D. Fittenghoff, T. Guo, D. Kim, C. Rose-Petruck, J. Squier, K. Yamakawa, K. Wilson, and C. P. J. Barty, Opt. Express **5**, 196 (1999).
[8] R. Wagner, S. Y. Chen, A. Maksimchuk, and D. Umstadter, Phys. Rev. Lett. **78**, 3125 (1997).
[9] J. Fuchs, J. C. Adams, F. Amiranoff, S. D. Baton, P. Gallant, L. Gremillet, A. Heron, J. C. Kieffer, G. Laval, G. Malka, J. L. Miquel, P. Mora, H. Pepin, and C. Rousseaux, Phys. Rev. Lett. **80**, 2326 (1998).
[10] B. Walker, B. Sheehy, L. F. Dimauro, P. Agostini, K. J. Schafer, and K. C. Kulander, Phys. Rev. Lett. **73**, 1227 (1994).
[11] M. V. Ammosov, N. B. Delone, and V. P. Krainov, Zh. Éksp. Teor. Fiz. **91**, 2008 (1986) [Sov. Phys. JETP **64**, 1191 (1986)].
[12] L. V. Keldysh, Zh. Éksp. Teor. Fiz. **47**, 1945 (1964) [Sov. Phys. JETP **20**, 1307 (1965)].
[13] L. D. Landau, *Quantum Mechanics: Non-Relativistic Theory* (Pergamon Press, New York, 1977), p. 293.
[14] B. M. Smirnov and M. I. Chibisov, Zh. Éksp. Teor. Fiz. **49**, 841 (1965) [Sov. Phys. JETP **22**, 585 (1966)].
[15] A. M. Perelomov, V. S. Popov, and M. V. Terent'ev, Zh. Éksp. Teor. Fiz. **50**, 1393 (1966) [Sov. Phys. JETP **23**, 924 (1966)].
[16] B. E. Sauer, S. Yoakum, L. Moorman, P. M. Koch, D. Richards, and P. A. Dando, Phys. Rev. Lett. **68**, 468 (1992).
[17] G. N. Gibson, G. Dunne, and K. J. Bergquist, Phys. Rev. Lett. **81**, 2663 (1998).
[18] R. W. Brankin, I. Gladwell, and L. F. Shampine (unpublished).
[19] R. L. Finney and D. R. Ostberg, *Elementary Differential Equations with Linear Algebra* (Addison-Wesley, Reading, MA, 1976), Chap. 7.
[20] H. J. Silverstone, B. G. Adams, J. Cizek, and P. Otto, Phys. Rev. Lett. **43**, 1498 (1979).
[21] See, for example, H. Reiss, Quantum Electron. **16**, 1 (1992).
[22] See V. P. Krainov, J. Phys. B **32**, 1607 (1999), and references therein.
[23] The first classical continuum model for photoelectrons in strong field-atom interactions is the ''simpleman's model.'' See H. B. van Linden van den Heuvell and H. G. Muller, in *Multiphoton Processes: Proceedings of the 4th International Conference on Multiphoton Processes*, edited by S. J. Smith and P. L. Knight (Cambridge University Press, New York, 1998), pp. 25–34; T. F. Gallagher, Phys. Rev. Lett. **61**, 2304 (1998). For a classical model treatment of continuum electrons in multiphoton ionization at 10^{13} W/cm^2 also see P. Agostini and G. Petite in *Atomic and Molecular Processes with Short Intense Laser Pulses*, edited by A. D. Bandrauk (Plenum Press, New York, 1988), pp. 135–143.
[24] P. B. Corkum, Phys. Rev. Lett. **71**, 1994 (1993).
[25] B. Sheehy, R. Lafon, M. Widmer, B. Walker, L. F. DiMauro, P. A. Agostini, and K. O. Kulander, Phys. Rev. A **58**, 3942 (1998).
[26] D. D. Meyerhofer, J. P. Knauer, S. J. McNaught, and C. I. Moore, J. Opt. Soc. Am. B **13**, 113 (1996).
[27] S. J. McNaught, J. P. Knauer, and D. D. Meyerhofer, Phys. Rev. A **58**, 1399 (1998).
[28] Th. Weber, M. Weckenbrock, A. Staudte, L. Spielberger, O. Jagutzki, V. Mergel, F. Afaneh, G. Urbasch, M. Vollmer, H. Giessen, and R. Drner, Phys. Rev. Lett. **84**, 443 (2000).